# *Planck* constraints on primordial non-Gaussianity

based on: arXiv:1303.5072

Sabino Matarrese

Physics & Astronomy Dept. "G. Galilei", University of Padova - Italy

*On behalf of the Planck collaboration*

# The scientific results that we present today are a product of the Planck Collaboration, including individuals from more than 100 scientific institutes in Europe, the USA and Canada

*Planck* is a project of the European Space Agency, with instruments provided by two scientific Consortia funded by ESA member states (in particular the lead countries: France and Italy) with contributions from NASA (USA), and telescope reflectors provided in a collaboration between ESA and a scientific Consortium led and funded by Denmark.

# Testable predictions of inflation

- Cosmological aspects
  - *Critical density Universe*
  - *Almost scale-invariant and nearly Gaussian, adiabatic density fluctuations*
  - *Almost scale-invariant stochastic background of relic gravitational waves*
- Particle physics aspects
  - *Nature of the inflaton*
  - *Inflation energy scale*

# Primordial non-Gaussianity: a new route to falsify Inflation ...

- Strongly non-Gaussian initial conditions studied in the eighties.
- New era with $f_{NL}$ models from inflation (Salopek & Bond 1991; Gangui et al. 1994: $f_{NL} \sim 10^{-2}$; Verde et al. 1999; Komatsu & Spergel 2001; Acquaviva et al. 2002; Maldacena 2002; + many models with (much) higher $f_{NL}$).
- Primordial NG emerged as a new "smoking gun" of (non-standard) inflation models, which complements the search for primordial GW.

# Simple-minded NG model ... has become reality

Many primordial (inflationary) models of non-Gaussianity can be represented in configuration space by the simple formula (Salopek & Bond 1990; Gangui et al. 1994; Verde et al. 1999; Komatsu & Spergel 2001)

$$\Phi = \phi_L + f_{NL} * ( \phi_L^2 - \langle \phi_L^2 \rangle ) + g_{NL} * ( \phi_L^3 - \langle \phi_L^2 \rangle \phi_L ) + \dots$$

where $\Phi$ is the large-scale gravitational potential (more precisely $\Phi = 3/5\ \zeta$ on superhorizon scales, where $\zeta$ is the gauge-invariant comovign curvature perturbation), $\phi_L$ its linear Gaussian contribution and $f_{NL}$ the dimensionless *non-linearity parameter* (or more generally *non-linearity function*). The percent of non-Gaussianity in CMB data implied by this model is

$$\text{NG \%} \sim 10^{-5}\ |f_{NL}|$$

$$\sim 10^{-10}\ |g_{NL}|$$

< $10^{-4}$ from CMB & LSS

< $10^{-4}$ from CMB & LSS

"non-Gaussianity = non-dog"
(Ya.B. Zel'dovich)

# NG CMB simulated maps

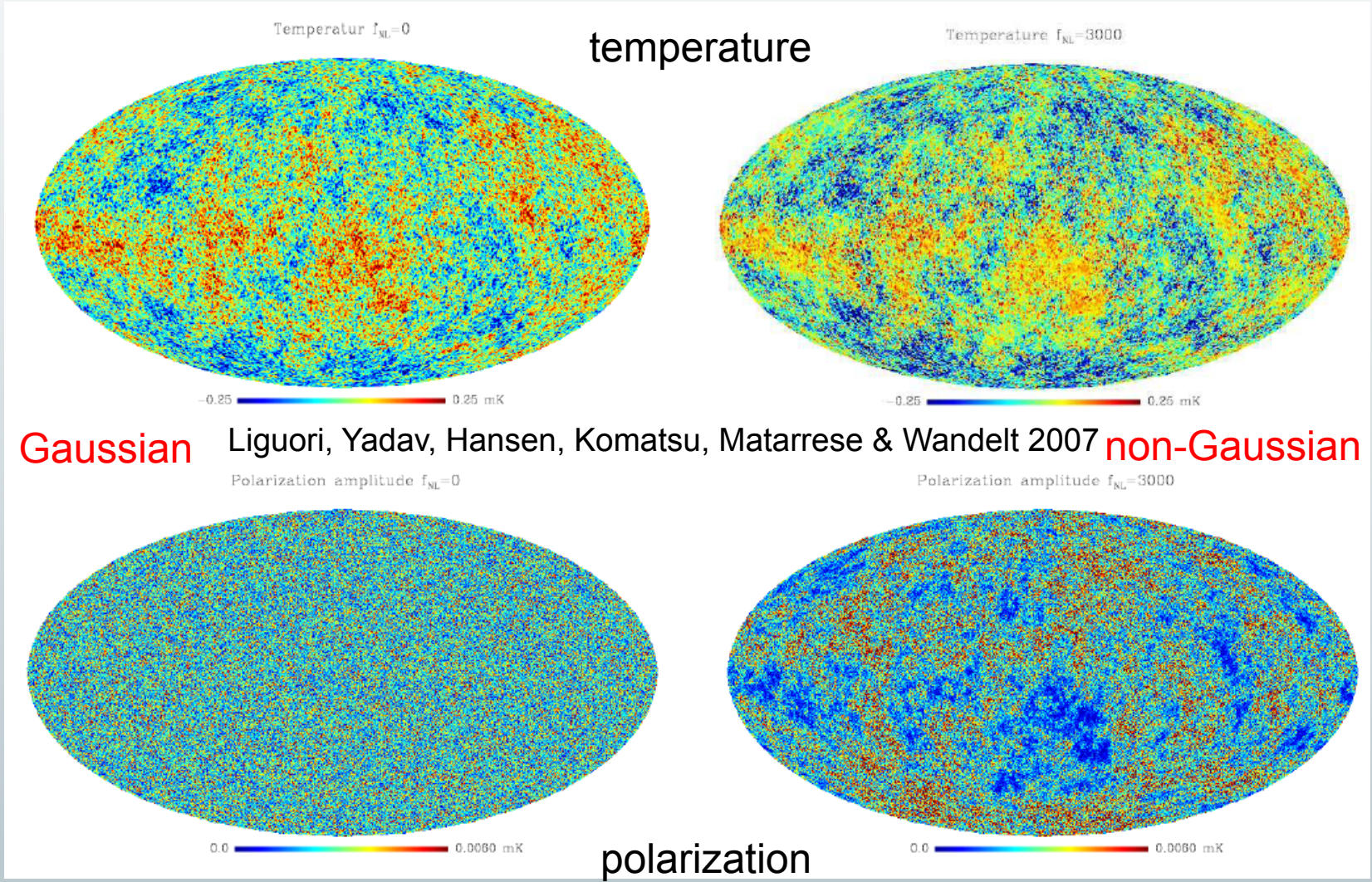

# Planck 2013 results XXIV: Scientific target

- Constrain (with high precision) and/or detect primordial non-Gaussianity (NG) as due to (non-standard) inflation
- NG amplitude and shape measure deviations from standard inflation, perturbation generating processes after inflation, initial state before inflation, ...
- We test: ***local, equilateral, orthogonal*** shapes (+ many more) for the bispectrum and constrain the primordial trispectrum (test of multi-field models) parameter $\tau_{NL}$

# the NG shape information

*... there are more shapes of non-Gaussianity (from inflation) than ... stars in the sky*

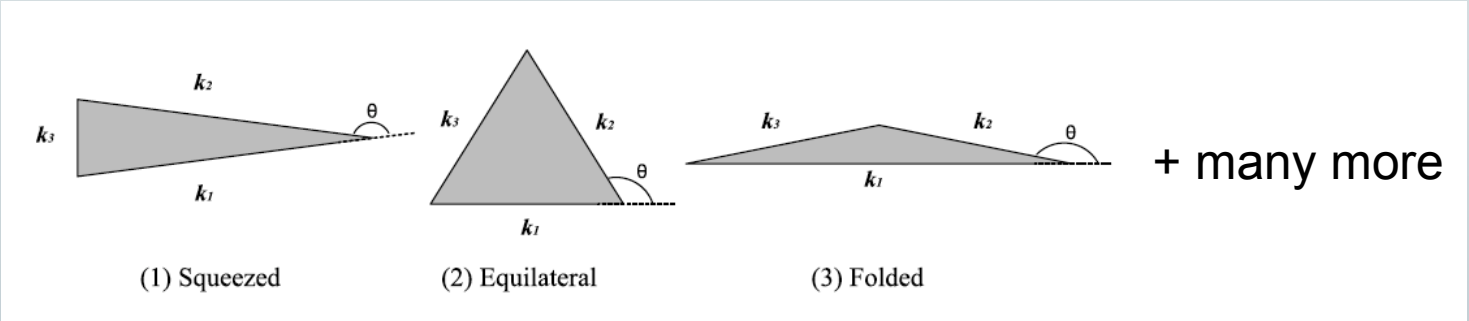

# CMB bispectrum

$$B^{m_1 m_2 m_3}_{\ell_1 \ell_2 \ell_3} \equiv \langle a_{\ell_1 m_1} a_{\ell_2 m_2} a_{\ell_3 m_3} \rangle$$

$$= \mathcal{G}^{\ell_1 \ell_2 \ell_3}_{m_1 m_2 m_3} \, b_{\ell_1 \ell_2 \ell_3}$$

Gaunt integrals

$$\mathcal{G}^{\ell_1 \ell_2 \ell_3}_{m_1 m_2 m_3} \equiv \int Y_{\ell_1 m_1}(\hat{\boldsymbol{n}}) \, Y_{\ell_2 m_2}(\hat{\boldsymbol{n}}) \, Y_{\ell_3 m_3}(\hat{\boldsymbol{n}}) \, d^2\hat{\boldsymbol{n}}$$

$$= h_{\ell_1 \ell_2 \ell_3} \begin{pmatrix} \ell_1 & \ell_2 & \ell_3 \\ m_1 & m_2 & m_3 \end{pmatrix},$$

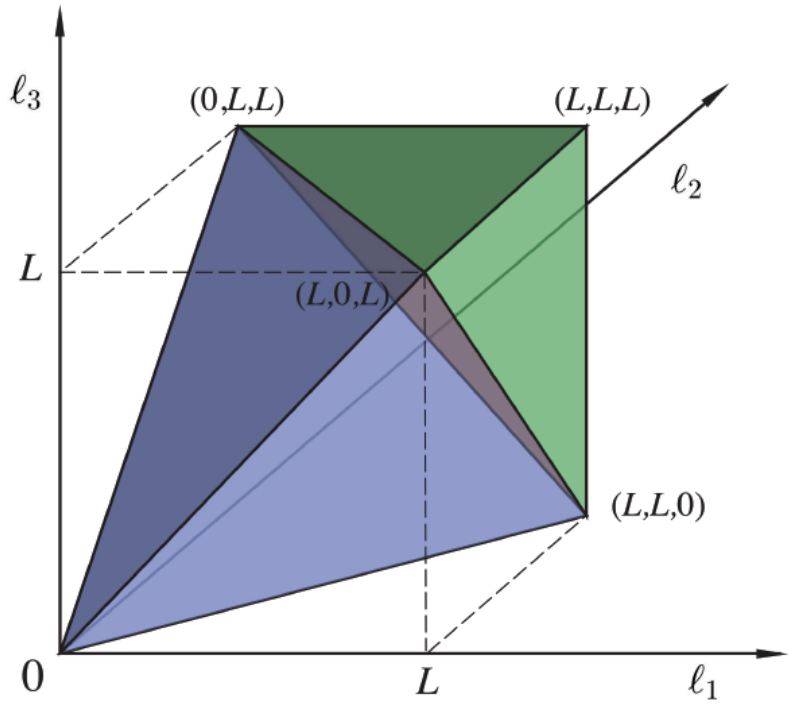


Triangle condition: $\ell_1 \leq \ell_2 + \ell_3$ for $\ell_1 \geq \ell_2, \ell_3$, +perms.

Parity condition: $\ell_1 + \ell_2 + \ell_3 = 2n, \quad n \in \mathbb{N},$

Resolution: $\ell_1, \ell_2, \ell_3 \leq \ell_{\max}, \quad \ell_1, \ell_2, \ell_3 \in \mathbb{N}.$

# Shapes

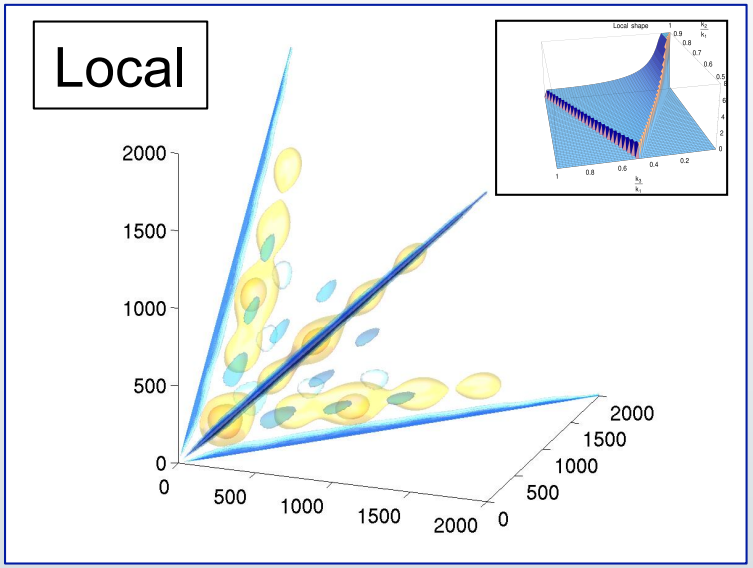
Local
2000
1500
1000
500
0
0
500
1000
1500
2000

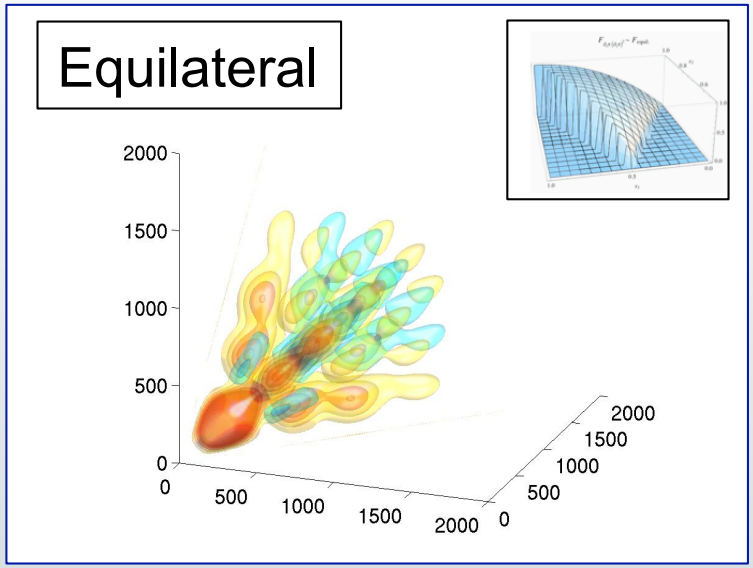
Equilateral
2000
1500
1000
500
0
0
500
1000
1500
2000

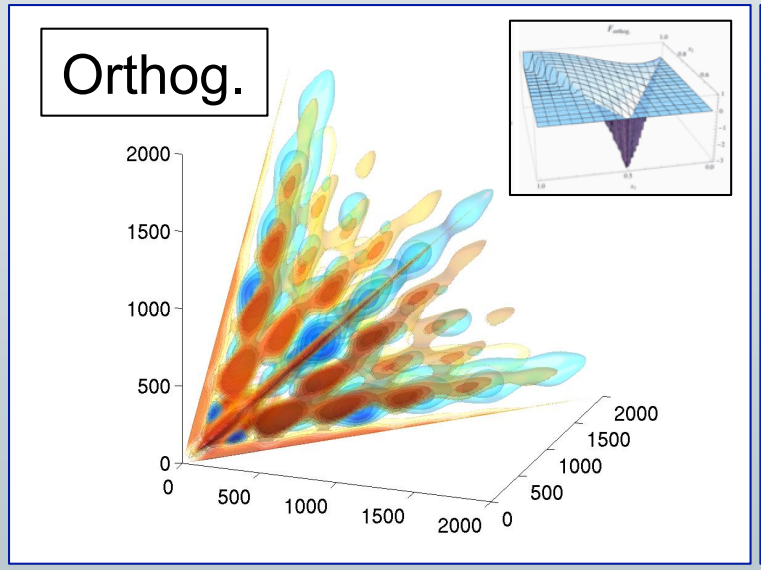
Orthog.
2000
1500
1000
500
0
0
500
1000
1500
2000

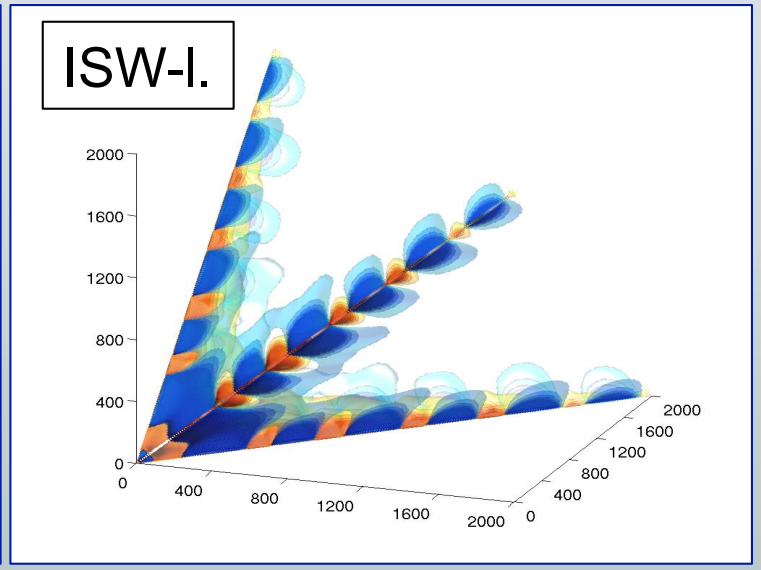
ISW-I.
2000
1600
1200
800
400
0
0
400
800
1200
1600
2000

# Bispectrum shapes

- ***local*** shape: Multi-field models, Curvaton, Ekpyrotic/cyclic, etc. ...

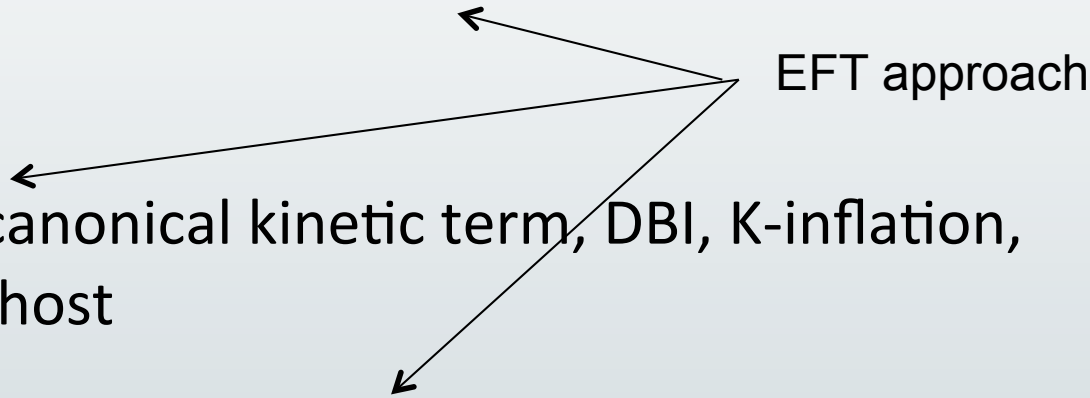


- ***equilateral*** shape: Non-canonical kinetic term, DBI, K-inflation, Higher-derivative terms, Ghost

- ***orthogonal*** shape: Distinguishes between variants of non-canonical kinetic term, higher-derivative interactions, Galilean inflation

- ***flat*** shape: non-Bunch-Davies initial state and higher-derivative interactions, models where a Galilean symmetry is imposed. The flat shape can be written in terms of equilateral and orthogonal

# Optimal $f_{NL}$ bispectrum estimator

$$\hat{f}_{NL} = \frac{1}{N}\sum B^{m_1 m_2 m_3}_{\ell_1 \ell_2 \ell_3}\left[\left(C^{-1}a\right)^{m_1}_{\ell_1}\left(C^{-1}a\right)^{m_2}_{\ell_2}\left(C^{-1}a\right)^{m_3}_{\ell_3} - 3C^{-1}_{\ell_1 m_1 \ell_2 m_2}\left(C^{-1}a\right)^{m_3}_{\ell_3}\right]$$

The theoretical template needs to be written in separable form. This can be done in different ways and *alternative implementations differ basically in terms of the separation technique adopted and of the projection domain*.

- KSW (Komatsu, Spergel & Wandelt 2003) separable template fitting + Skew-$C_l$ extension (Munshi & Heavens 2010)
- Binned bispectrum (Bucher, Van Tent & Carvalho 2009) → see B. Racine talk
- Modal expansion (Fergusson, Liguori & Shellard 2009)

*Sub-optimal estimators also applied:*
*Wavelet decomposition (Martinez-Gonzalez et al. 2002; Curto et al. 2009) &*
*Minkowski Functionals (Ducout et al. 2013)*

# Optimal $f_{NL}$ bispectrum estimator

$$\hat{f}_{NL} = \frac{1}{N}\sum B^{m_1 m_2 m_3}_{\ell_1 \ell_2 \ell_3}\left(C^{-1}a\right)^{m_1}_{\ell_1}\left(C^{-1}a\right)^{m_2}_{\ell_2}\left(C^{-1}a\right)^{m_3}_{\ell_3} - 3C^{-1}_{\ell_1 m_1 \ell_2 m_2}\left(C^{-1}a\right)^{m_3}_{\ell_3}$$

Leaving aside complications coming from breaking of statistical isotropy (sky-cut, noise…), one can see that we are extracting the three point Function from the data and fitting theoretical bispectrum templates to it

$$\hat{f}_{NL} = \frac{1}{N}\sum_{\ell_i m_i} B^{m_1 m_2 m_3}_{\ell_1 \ell_2 \ell_3}\frac{a^{m_1}_{\ell_1}}{C_{\ell_1}}\frac{a^{m_2}_{\ell_2}}{C_{\ell_2}}\frac{a^{m_3}_{\ell_3}}{C_{\ell_3}}$$

A brute force implementation scales like $\ell^5_{\max}$. Unfeasible at Planck (or WMAP) resolution.

Can achieve massive speed improvement ($\ell^3_{\max}$ scaling) if the reduced bispectrum is *separable* (Komatsu, Spergel, Wandelt 2003)

$$b_{\ell_1\ell_2\ell_3} = \sum_{ijk} X^i_{\ell_1} Y^j_{\ell_2} Z^k_{\ell_3} \Rightarrow B^{m_1 m_2 m_3}_{\ell_1\ell_2\ell_3} = b_{\ell_1\ell_2\ell_3}\int Y^{m_1}_{\ell_1}(\Omega) Y^{m_2}_{\ell_2}(\Omega) Y^{m_3}_{\ell_3}(\Omega)$$

# Going to higher order?

Verde, Jimenez, Alvarez-Gaume, Heavens & Matarrese 2013

$$\mathcal{P}(a|f_{\rm NL}) = \frac{(\det C^{-1})^{1/2}}{(2\pi)^{n/2}} \exp\left[-\frac{1}{2}\sum_{\ell\ell' mm'} a_\ell^{*m}(C^{-1})_{\ell m\ell' m'} a_{\ell'}^{m'})\right] \times$$

$$\left\{1 + \frac{1}{6}\sum_{\text{all } \ell_i m_j} \langle a_{\ell_1}^{m_1} a_{\ell_2}^{m_2} a_{\ell_3}^{m_3}\rangle \left[(C^{-1}a)_{\ell_1}^{m_1}(C^{-1}a)_{\ell_2}^{m_2}(C^{-1}a)_{\ell_3}^{m_3} - 3(C^{-1})_{l_1,l_2}^{m_1 m_2}(C^{-1}a)_{l_3}^{m_3}\right] + \right.$$

$$\frac{1}{24}\sum_{\text{all } \ell m} \langle a_{\ell_1}^{m_1} a_{\ell_2}^{m_2} a_{\ell_3}^{m_3} a_{\ell_4}^{m_4}\rangle \left[3(C^{-1})_{\ell_1\ell_2}^{m_1 m_2}(C^{-1})_{\ell_3,\ell_4}^{m_3 m_4}\right.$$

$$\left. -6(C^{-1})_{\ell_1,\ell_2}^{m_1 m_2}(C^{-1}a)_{\ell_3}^{m_3}(C^{-1}a)_{\ell_4}^{m_4} + (C^{-1}a)_{\ell_1}^{m_1}(C^{-1}a)_{\ell_2}^{m_2}(C^{-1}a)_{\ell_3}^{m_3}(C^{-1}a)_{\ell_4}^{m_4}\right] +$$

$$\frac{1}{72}\sum_{l_1,\ldots,l_6} \langle a_{\ell_1}^{m_1} a_{\ell_2}^{m_2} a_{\ell_3}^{m_3}\rangle\langle a_{\ell_4}^{m_4} a_{\ell_5}^{m_5} a_{\ell_6}^{m_6}\rangle \left[(C^{-1}a)_{\ell_1}^{m_1}(C^{-1}a)_{\ell_2}^{m_2}(C^{-1}a)_{\ell_3}^{m_3}(C^{-1}a)_{\ell_4}^{m_4}(C^{-1}a)_{\ell_5}^{m_5}(C^{-1}a)_{\ell_6}^{m_6}\right.$$

$$-15(C^{-1})_{\ell_1\ell_2}^{m_1 m_2}(C^{-1}a)_{\ell_3}^{m_3}(C^{-1}a)_{\ell_4}^{m_4}(C^{-1}a)_{\ell_5}^{m_5}(C^{-1}a)_{\ell_6}^{m_6}$$

$$\left.\left. -15(C^{-1})_{\ell_1\ell_2}^{m_1 m_2}(C^{-1})_{\ell_3\ell_4}^{m_3 m_4}(C^{-1})_{\ell_5\ell_6}^{m_5 m_6} + 45(C^{-1})_{\ell_1\ell_2}^{m_1 m_2}(C^{-1})_{\ell_3\ell_4}^{m_3 m_4}(C^{-1}a)_{\ell_5}^{m_5}(C^{-1}a)_{\ell_6}^{m_6}\right]\right\}$$

It may become important if we want to detect NG in observables where $f_{NL}$ is large (e.g. in high-redshift probes) and/or if both $f_{NL}$ (→ leading order bispectrum) and $g_{NL}$ (leading-order trispectrum) are both depending on the same underlying physical coupling constant that we aim at determining.

# Simulation challenges

To participate in the analysis all estimators have to pass a suite of challenges:

- *Map-by-map agreement of estimators*
- *Gaussian simulations*
- *Non-Gaussian simulations*
- *Robust to foreground residuals*
- *Blind challenge of recovering unknown non-Gaussianity from a realistically simulated map (FFP6)*

# Comparison between pipelines

## Local

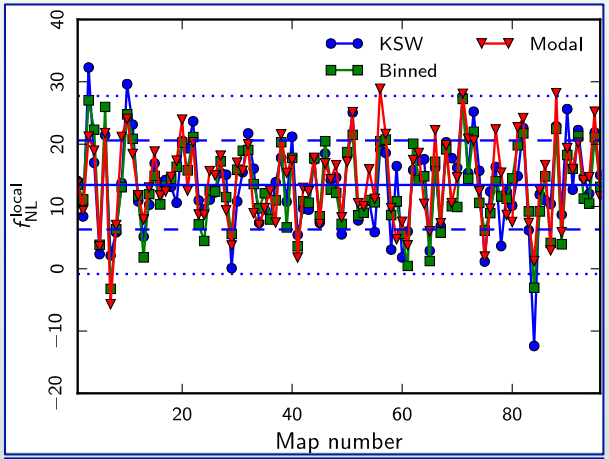


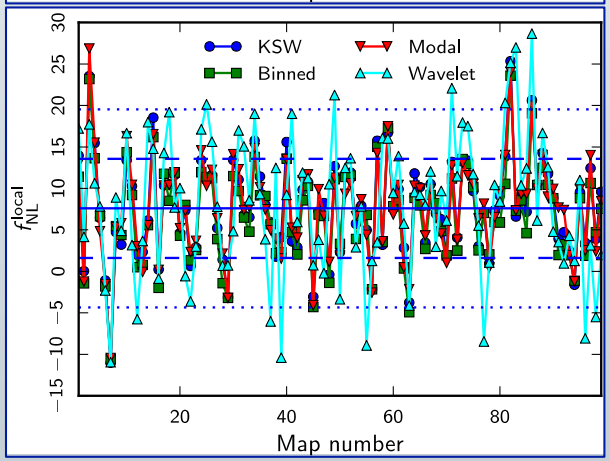


## Equilateral

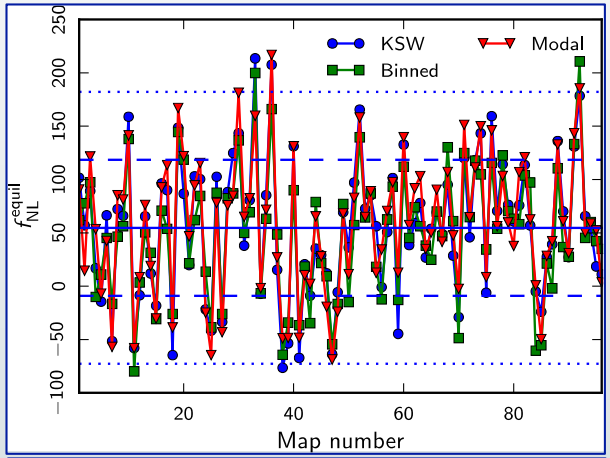


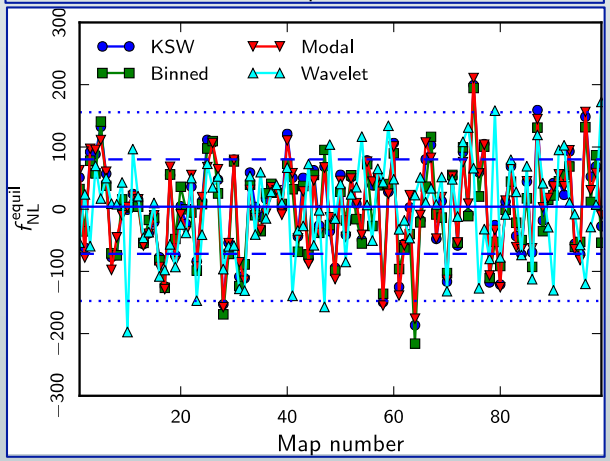


## Orthogonal

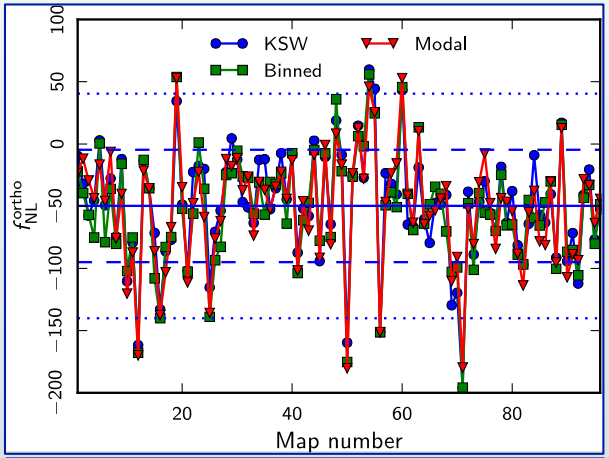


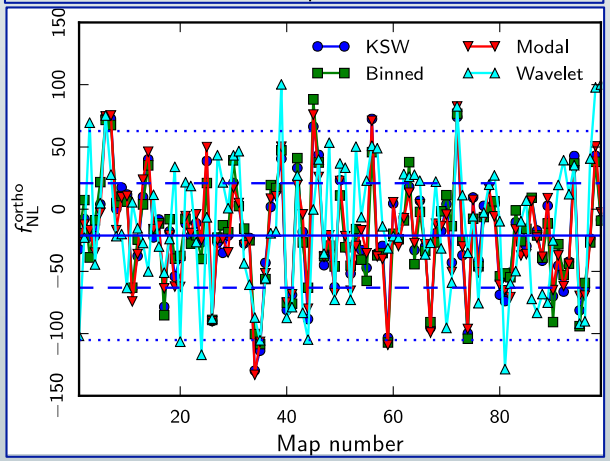


- Top row: wave expansion, NG sims (loc+eq+ortho, anis. noise, U73 mask)
- Bottom row: polynomial expansion, lensed FFP6 sims

# Modes from *Planck* data

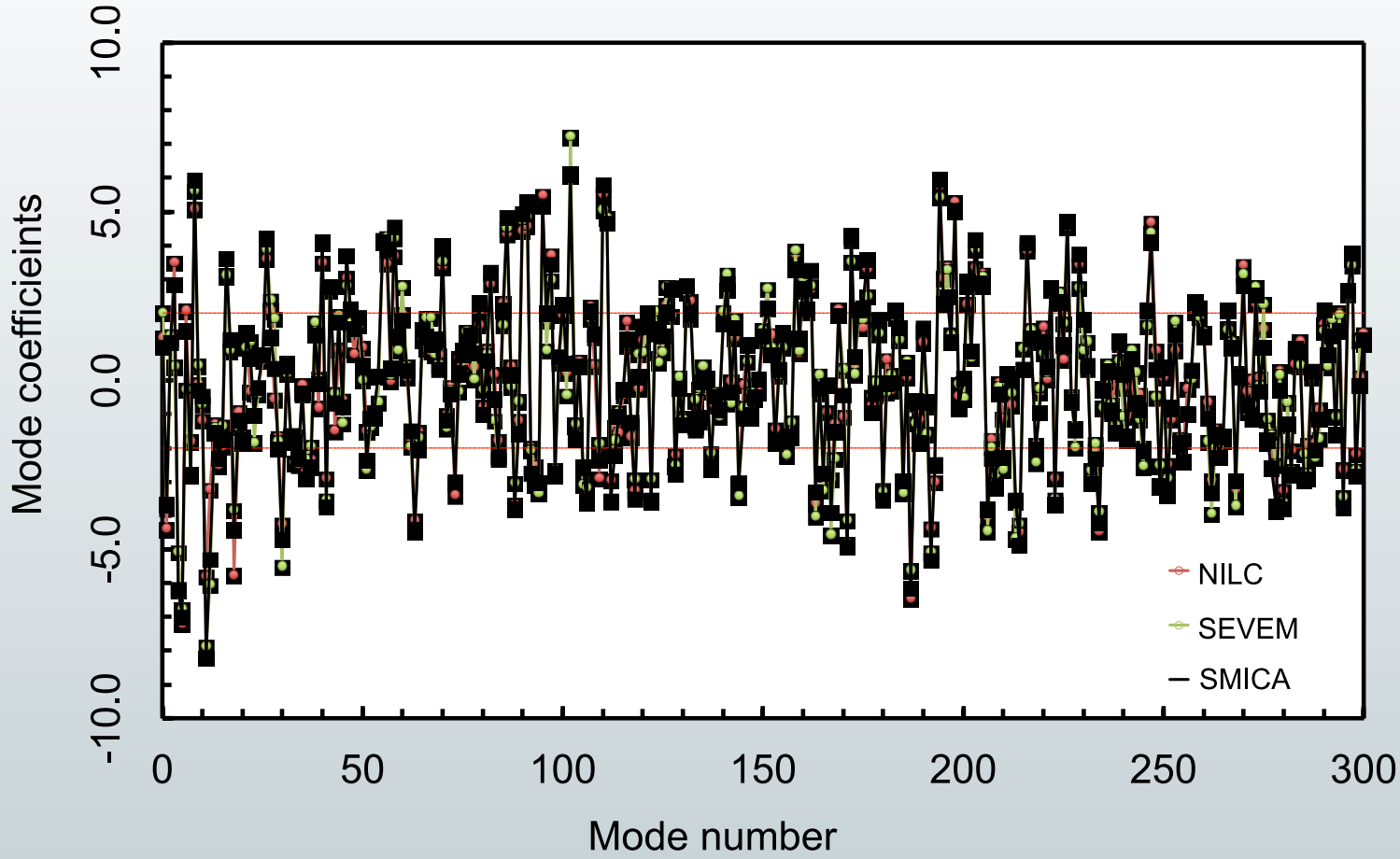


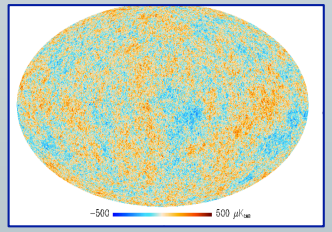

$$(\beta_0, \beta_1, \cdot \quad, \beta_n)$$

# The *Planck* NG analysis passed an extensive validation campaign

- Different estimators agree: *KSW (Komatsu, Spergel & Wandelt 2003), Modal (Fergusson, Liguori & Shellard, 2009), Binned (Bucher, van Tent & Carvalho 2009), Skew-$C_l$ (Munshi & Heavens 2010), Minkowski Functionals (Ducout et al. 2012)*

- Multiple foreground cleaning methods agree*: SMICA, NILC, SEVEM, (C-R)*

- Negligible impact of foreground residuals

- Null tests pass

- Consistent...*: Resolution dependence, Frequency dependence, Mask dependence*

# The *Planck* modal bispectrum

SMICA

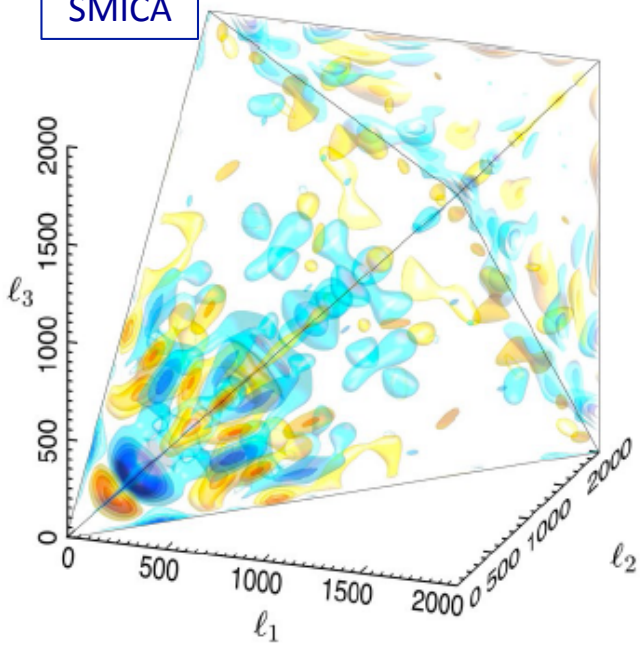


NILC

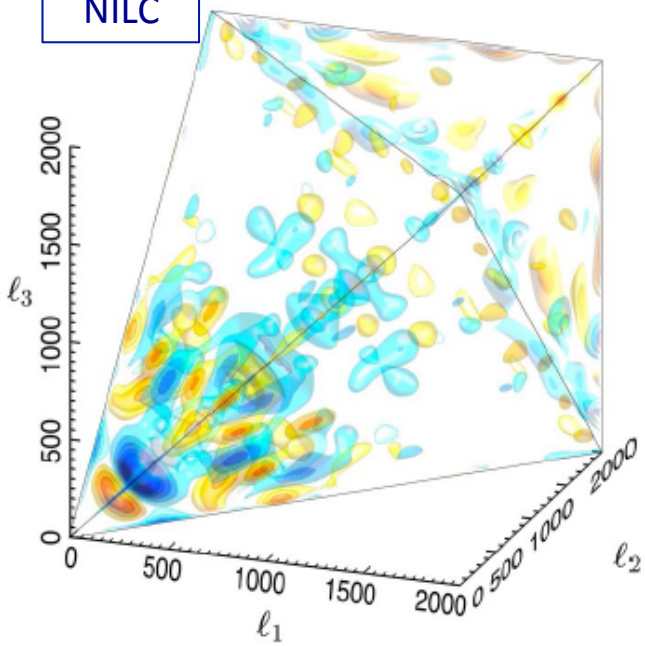


SEVEM

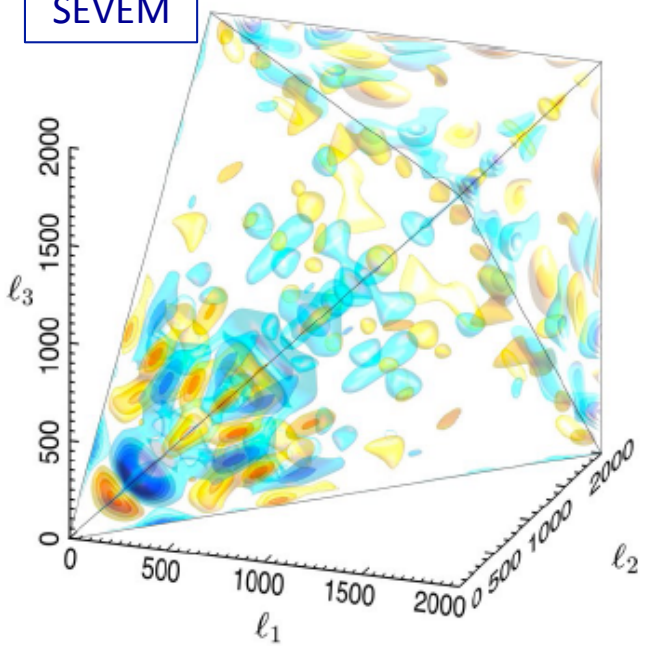


Full 3D CMB bispectrum recovered from the *Planck* foreground-cleaned maps, including SMICA, NILC and SEVEM, using hybrid Fourier mode coefficients, These are plotted in three-dimensions with multipole coordinates ($l_1$,$l_2$,$l_3$) on the tetrahedral domain out to $l_{max}$ = 2000. Several density contours are plotted with red positive and blue negative. The bispectra extracted from the different foreground-separated maps are almost indistinguishable

# Consistency with *WMAP*

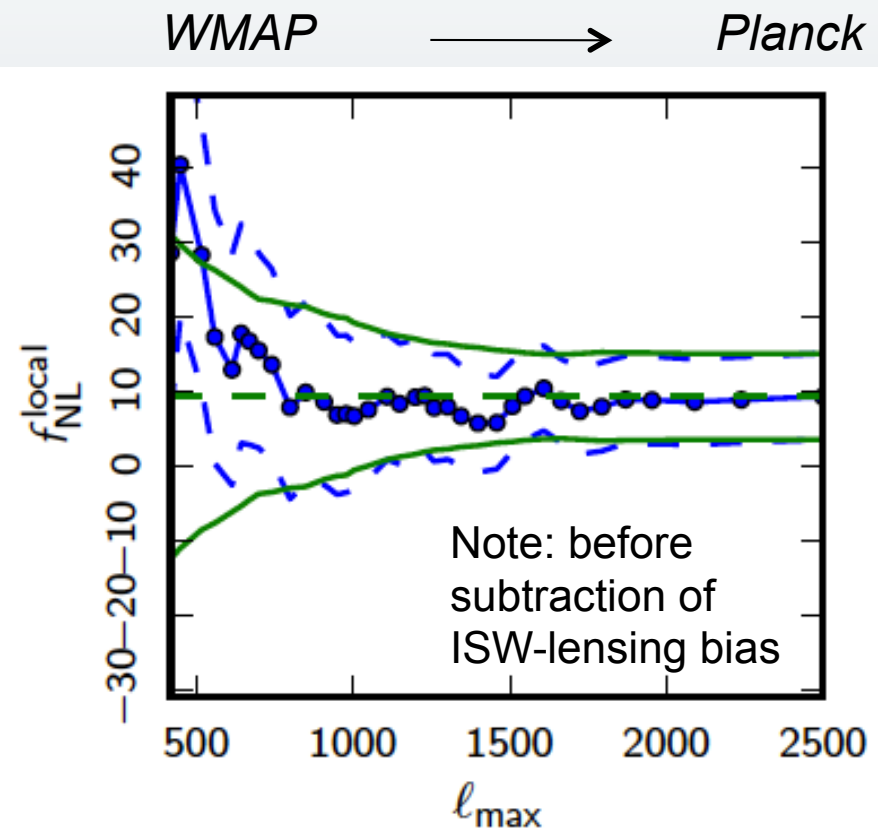


- By limiting the analysis to large scales (low l), we make contact with *WMAP9* ($f_{NL}^{local} = 37.2 \pm 20$)
- *Planck* now rules out the *WMAP* central value by ≈ 6 sigmas.

# ISW-lensing bispectrum from *Planck*

The coupling between weak lensing and Integrated Sachs-Wolfe (ISW) effects is the leading contamination to local NG. We have detected the ISW lensing bispectrum with a significance of 2.6 σ

| | SMICA | NILC | SEVEM | C-R |
|---|---|---|---|---|
| KSW . . . . . | 0.81 ± 0.31 | 0.85 ± 0.32 | 0.68 ± 0.32 | 0.75 ± 0.32 |
| Binned . . . . | 0.91 ± 0.37 | 1.03 ± 0.37 | 0.83 ± 0.39 | 0.80 ± 0.40 |
| Modal . . . . | 0.77 ± 0.37 | 0.93 ± 0.37 | 0.60 ± 0.37 | 0.68 ± 0.39 |

Results for the amplitude of the ISW-lensing bispectrum from the SMICA, NILC, SEVEM, and C-R foreground-cleaned maps, for the KSW, binned, and modal (polynomial) estimators; error bars are 68% CL.

| | SMICA | NILC | SEVEM | C-R |
|---|---|---|---|---|
| Local . . . . . | 7.1 | 7.0 | 7.1 | 6.0 |
| Equilateral . . . . . | 0.4 | 0.5 | 0.4 | 1.4 |
| Orthogonal . . . . . | −22 | −21 | −21 | −19 |

The bias in the three primordial fNL parameters due to the ISW-lensing signal for the 4 component-separation methods.

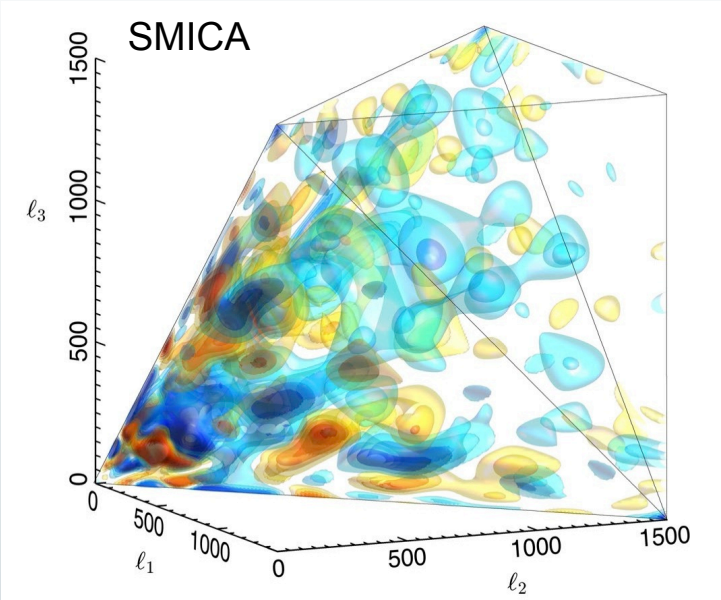


Skew-$C_l$ detection of ISW-lensing signal

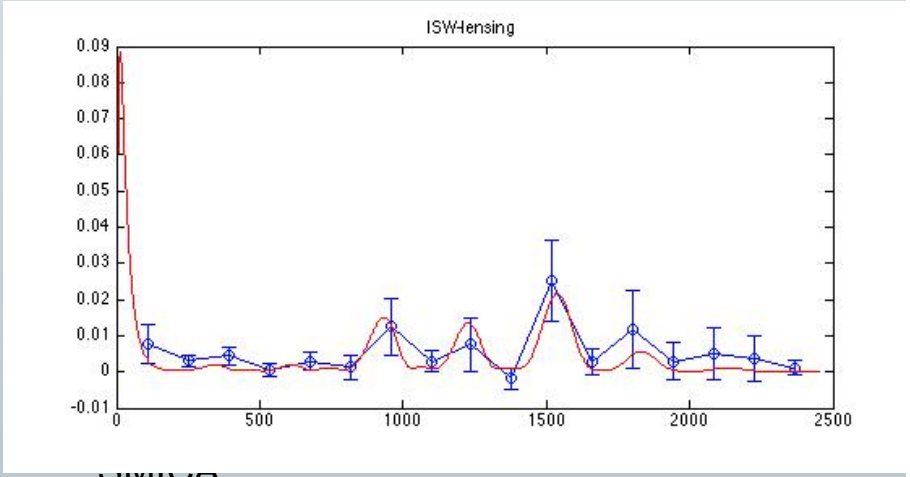


SMICA

# Point-sources (Poissonian) bispectrum

- Results for the amplitude of the point-source (Poisson) bispectrum (in dimensionless units of $10^{-29}$) from the SMICA, NILC, SEVEM, and C-R foreground-cleaned maps, for the KSW, binned, and modal (polynomial) estimators; error bars are 68% CL. Note that the KSW and binned estimators use $l_{max} = 2500$, while the modal estimator has $l_{max} = 2000$.

| | SMICA | NILC | SEVEM | C–R |
|---|---|---|---|---|
| KSW . . . . . | 7.7 ± 1.5 | 9.2 ± 1.7 | 7.6 ± 1.7 | 1.1 ± 5.1 |
| Binned . . . . | 7.7 ± 1.6 | 8.2 ± 1.6 | 7.5 ± 1.7 | 0.9 ± 4.8 |
| Modal . . . . . | 10 ± 3 | 11 ± 3 | 10 ± 3 | 0.5 ± 6 |

Skew-$C_l$ detection of Poissonian point-source bispectrum

Skew-$C_l$s are optimised statistics which retain information on the nature of any NG (Munshi & Heavens 2010)

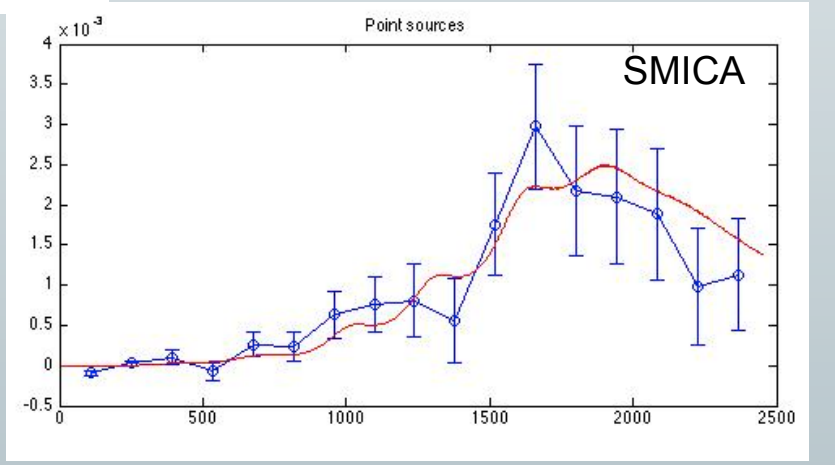

# Results for 3 fundamental shapes (KSW)

- Results for the $f_{NL}$ parameters of the primordial local, equilateral, and orthogonal shapes, determined by the KSW estimator from the SMICA foreground-cleaned map. Both independent single-shape results and results marginalized over the point-source bispectrum and with the ISW-lensing bias subtracted are reported; error bars are 68% CL.

| | Independent | ISW-lensing subtracted |
|---|---|---|
| | KSW | KSW |
| SMICA | | |
| Local . . . . . | $9.8 \pm 5.8$ | $\mathbf{2.7 \pm 5.8}$ |
| Equilateral . . . . . | $-37 \pm 75$ | $\mathbf{-42 \pm 75}$ |
| Orthogonal . . . . . | $-46 \pm 39$ | $\mathbf{-25 \pm 39}$ |

- Union Mask U73 (73% sky coverage) used throughout. Diffusive inpainting pre-filtering procedure applied.

# Results for 3 fundamental shapes

- Results for the $f_{NL}$ parameters of the primordial local, equilateral, and orthogonal shapes, determined by the KSW, binned and modal estimators from the SMICA, NILC, SEVEM, and C-R foreground-cleaned maps. Both independent single-shape results and results marginalized over the point-source bispectrum and with the ISW-lensing bias subtracted are reported; error bars are 68% CL.

| | Independent | | | ISW-lensing subtracted | | |
|---|---|---|---|---|---|---|
| | KSW | Binned | Modal | KSW | Binned | Modal |
| **SMICA** | | | | | | |
| Local | 9.8 ± 5.8 | 9.2 ± 5.9 | 8.3 ± 5.9 | **2.7 ± 5.8** | 2.2 ± 5.9 | 1.6 ± 6.0 |
| Equilateral | −37 ± 75 | −20 ± 73 | −20 ± 77 | **−42 ± 75** | −25 ± 73 | −20 ± 77 |
| Orthogonal | −46 ± 39 | −39 ± 41 | −36 ± 41 | **−25 ± 39** | −17 ± 41 | −14 ± 42 |
| **NILC** | | | | | | |
| Local | 11.6 ± 5.8 | 10.5 ± 5.8 | 9.4 ± 5.9 | 4.5 ± 5.8 | 3.6 ± 5.8 | 2.7 ± 6.0 |
| Equilateral | −41 ± 76 | −31 ± 73 | −20 ± 76 | −48 ± 76 | −38 ± 73 | −20 ± 78 |
| Orthogonal | −74 ± 40 | −62 ± 41 | −60 ± 40 | −53 ± 40 | −41 ± 41 | −37 ± 43 |
| **SEVEM** | | | | | | |
| Local | 10.5 ± 5.9 | 10.1 ± 6.2 | 9.4 ± 6.0 | 3.4 ± 5.9 | 3.2 ± 6.2 | 2.6 ± 6.0 |
| Equilateral | −32 ± 76 | −21 ± 73 | −13 ± 77 | −36 ± 76 | −25 ± 73 | −13 ± 78 |
| Orthogonal | −34 ± 40 | −30 ± 42 | −24 ± 42 | −14 ± 40 | −9 ± 42 | −2 ± 42 |
| **C-R** | | | | | | |
| Local | 12.4 ± 6.0 | 11.3 ± 5.9 | 10.9 ± 5.9 | 6.4 ± 6.0 | 5.5 ± 5.9 | 5.1 ± 5.9 |
| Equilateral | −60 ± 79 | −52 ± 74 | −33 ± 78 | −62 ± 79 | −55 ± 74 | −32 ± 78 |
| Orthogonal | −76 ± 42 | −60 ± 42 | −63 ± 42 | −57 ± 42 | −41 ± 42 | −42 ± 42 |

# $f_{NL}$ from *Planck* data

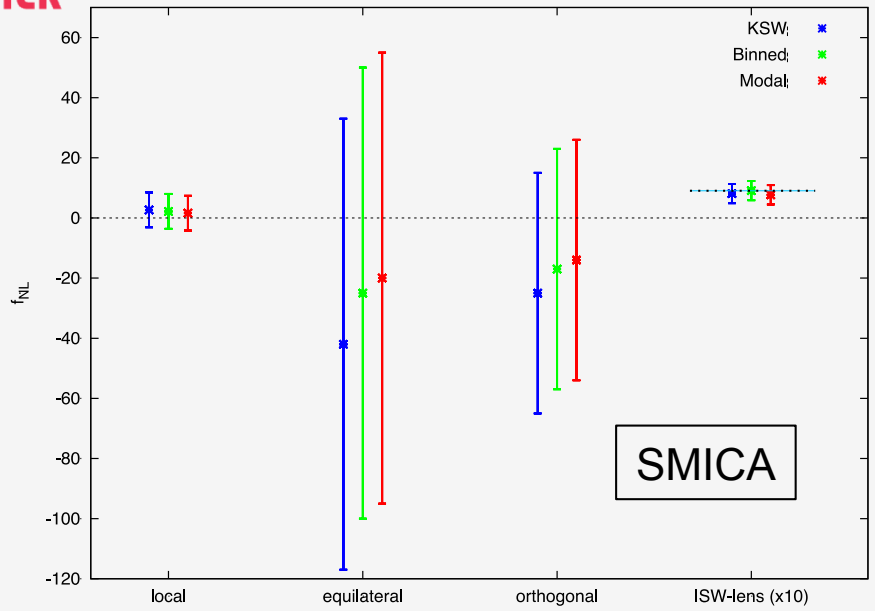


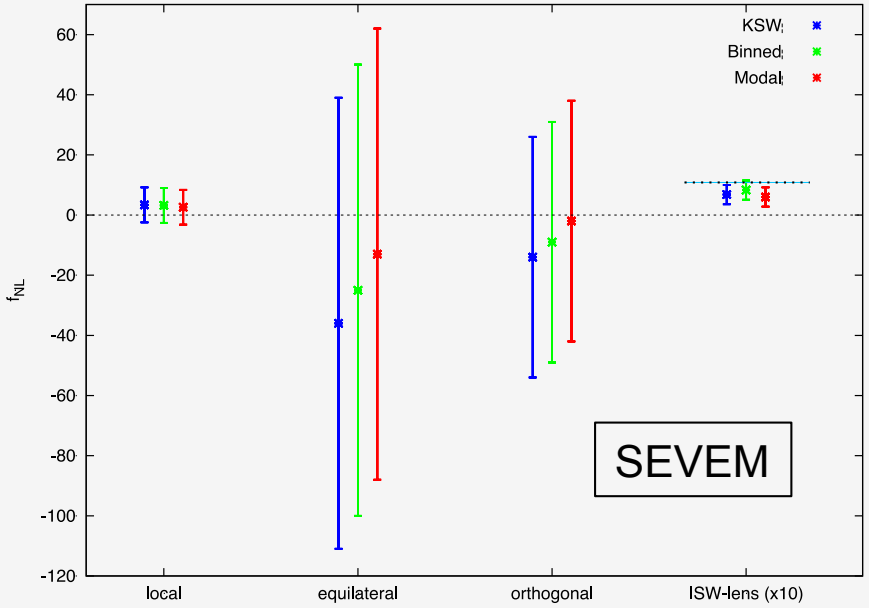


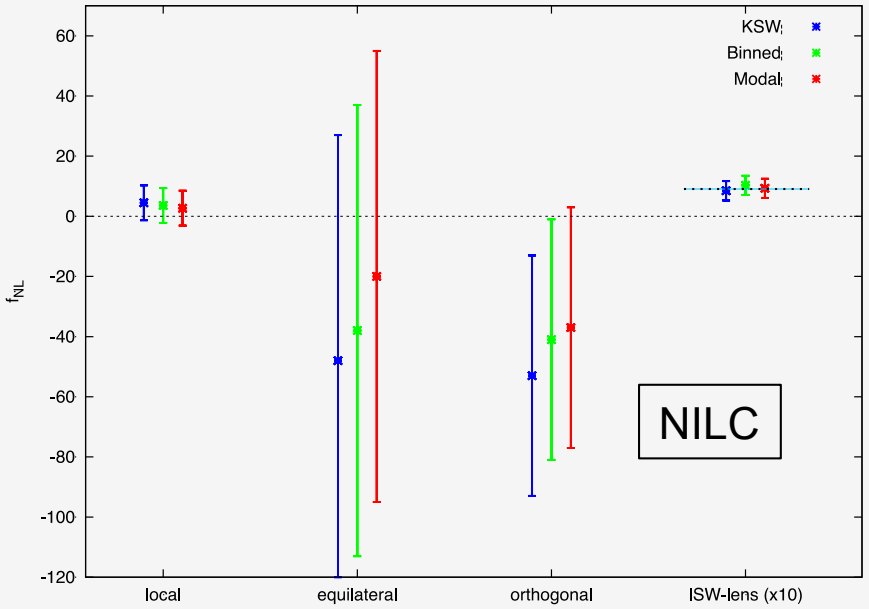


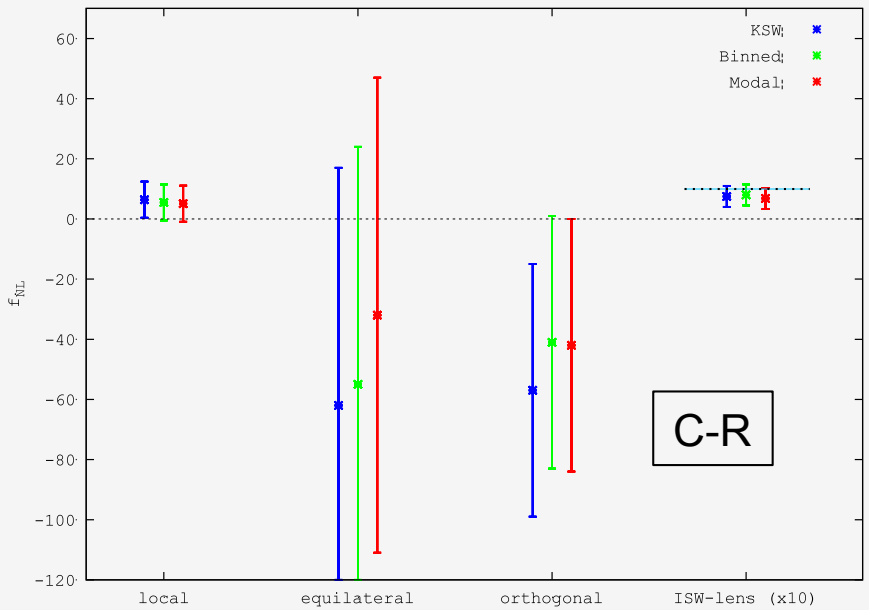

# The *Planck* modal bispectrum

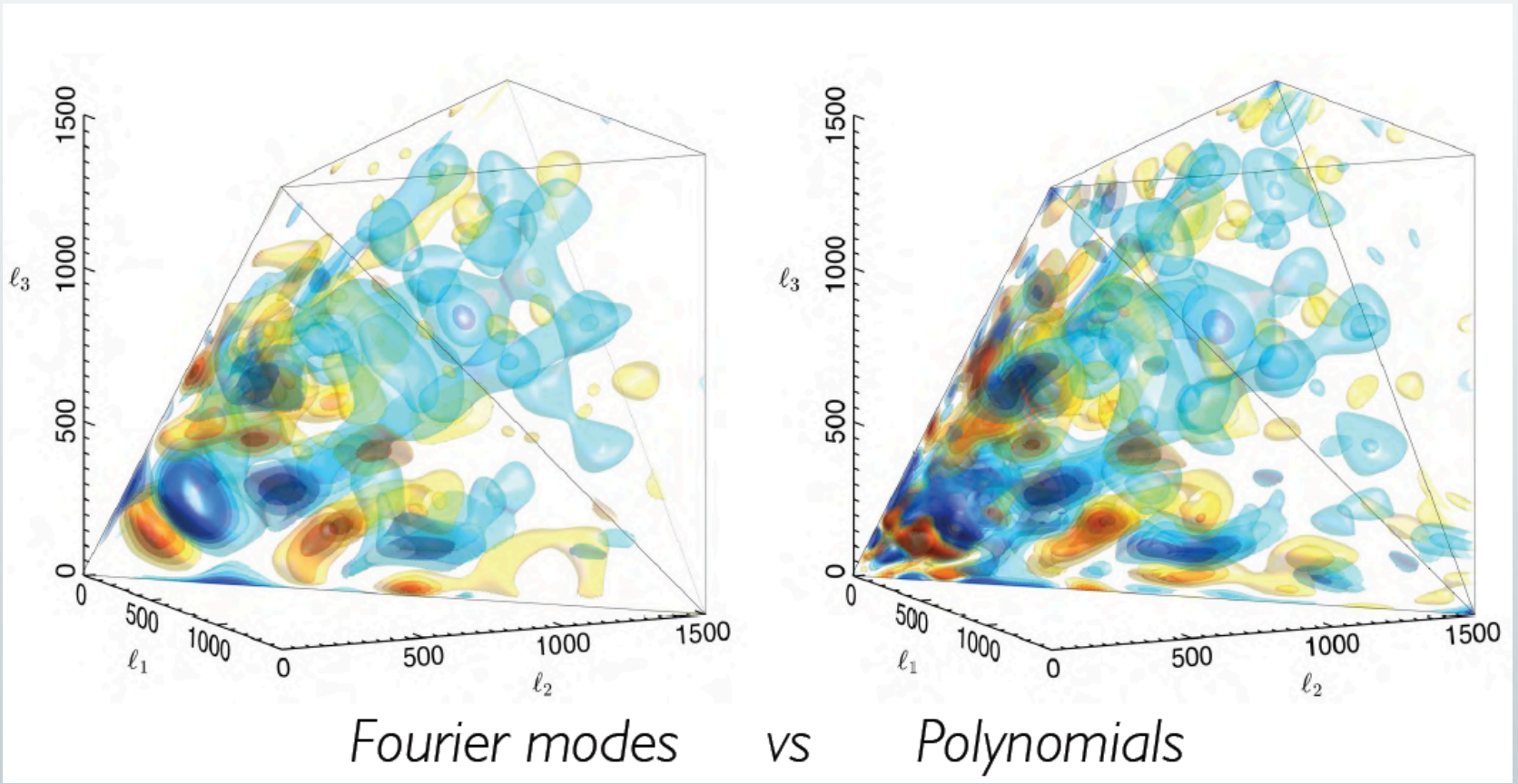

# Results with sub-optimal estimators

## ➢ Wavelets

| | Independent Wavelets | ISW-lensing subtracted Wavelets |
|---|---|---|
| SMICA | | |
| Local . . . . . | 10 ± 8.5 | 0.9 ± 8.5 |
| Equilateral . . . . . | 89 ± 84 | 90 ± 84 |
| Orthogonal . . . . . | −73 ± 52 | −45 ± 52 |

Results for $f_{NL}$ parameters of local, equilateral, and orthogonal shapes, determined by the suboptimal wavelet estimator (as described in Martinez-Gonzalez et al. 2002; Curto et al. 2009) from the SMICA foreground-cleaned map. Both independent single-shape results and results marginalized over the point source bispectrum and with the ISW-lensing bias subtracted are reported; error bars are 68% CL. Our current wavelets pipeline performs slightly worse in terms of error bars and correlation to primordial templates than other bispectrum estimators, but it provides an independent cross-check of other techniques.

## ➢ Minkowski Functionals

| | $f_{NL}^{local}$ | Source | Corresponding $\Delta f_{NL}^{local}$ |
|---|---|---|---|
| Raw map | 19.1 ± 19.3 | | – |
| Lensing subtracted | 8.5 ± 20.5 | Lensing | +10.6 |
| Lensing+PS subtracted | 7.7 ± 20.3 | Point sources | +0.8 |
| Lensing+CIB subtracted | 7.5 ± 20.5 | CIB | +1.0 |
| Lensing+SZ subtracted | 6.0 ± 20.4 | SZ | +2.5 |
| All subtracted | 4.2 ± 20.5 | All | +14.9 |

Minkowski Functionals estimates of $f_{NL}$ local (method as in Ducout et al. 2013) obtained with MFs. Foreground and secondary effects evaluated in terms of $f_{NL}$ local. Results for SMICA at $N_{side}$ = 1024 and $l_{max}$ = 2000.

# Standard inflation vs. NG

Standard inflation:

- *single scalar field*
- *canonical kinetic term*
- *slow-roll dynamics*
- *Bunch-Davies initiual vacuum state*
- *standard Einstein gravity*

→ no (presently) detectable primordial NG

# non-standard shapes: excited initial states

Non-Bunch-Davies vacua from trans-Planckian effects or features

Five exemplar flattened models constrained

NBD case

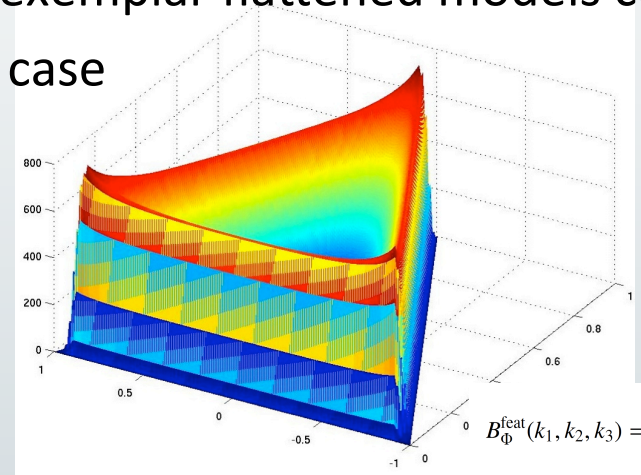

$$B_{\Phi}^{\rm feat}(k_1,k_2,k_3)=\frac{6A^2 f_{\rm NL}^{\rm feat}}{(k_1k_2k_3)^2}\sin\left[\frac{2\pi(k_1+k_2+k_3)}{3k_{\rm c}}+\phi\right]$$

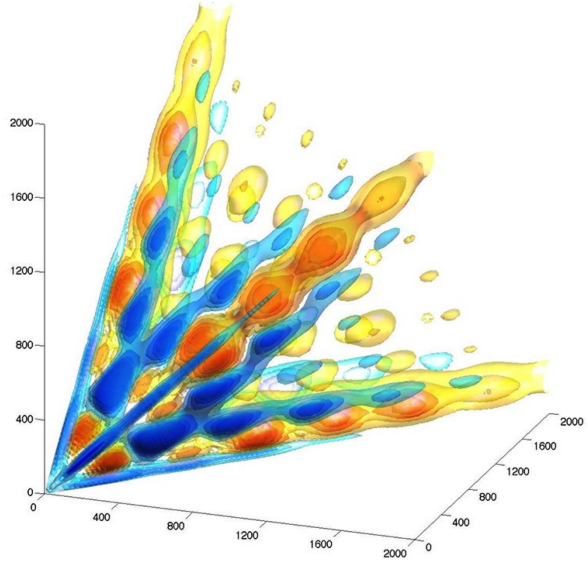

| Flattened model (Eq. number) | Raw $f_{\rm NL}$ | Clean $f_{\rm NL}$ | $\Delta f_{\rm NL}$ | $\sigma$ | Clean $\sigma$ |
|---|---|---|---|---|---|
| Flat model (13) | 70 | 37 | 77 | 0.9 | 0.5 |
| Non-Bunch-Davies (NBD) | 178 | 155 | 78 | 2.2 | 2.0 |
| Single-field NBD1 flattened (14) | 31 | 19 | 13 | 2.4 | 1.4 |
| Single-field NBD2 squeezed (14) | 0.8 | 0.2 | 0.4 | 1.8 | 0.5 |
| Non-canonical NBD3 (15) | 13 | 9.6 | 9.7 | 1.3 | 1.0 |
| Vector model $L=1$ (19) | −18 | −4.6 | 47 | −0.4 | −0.1 |
| Vector model $L=2$ (19) | 2.8 | −0.4 | 2.9 | 1.0 | −0.1 |

➢ … but beware of “look elsewhere effect!”

# 3s hint of oscillatory NG?

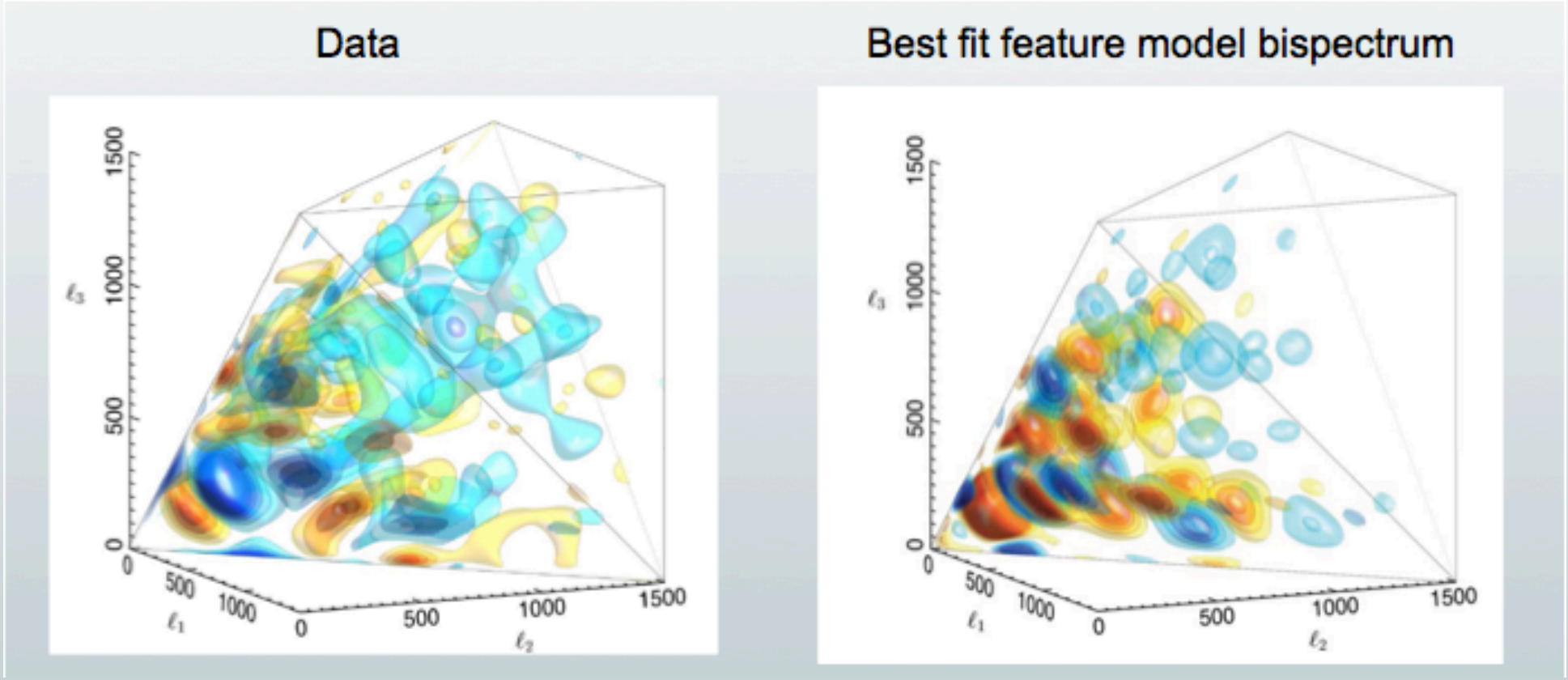


- Significance of best-fit shape goes down to < 2σ when "look elsewhere" effect is taken into account

# non-standard shapes: models of inflation with primordial gauge fields

| Flattened model (Eq. number) | Raw $f_{NL}$ | Clean $f_{NL}$ | $\Delta f_{NL}$ | $\sigma$ | Clean $\sigma$ |
|---|---|---|---|---|---|
| Flat model (13) | 70 | 37 | 77 | 0.9 | 0.5 |
| Non-Bunch-Davies (NBD) | 178 | 155 | 78 | 2.2 | 2.0 |
| Single-field NBD1 flattened (14) | 31 | 19 | 13 | 2.4 | 1.4 |
| Single-field NBD2 squeezed (14) | 0.8 | 0.2 | 0.4 | 1.8 | 0.5 |
| Non-canonical NBD3 (15) | 13 | 9.6 | 9.7 | 1.3 | 1.0 |
| Vector model $L = 1$ (19) | −18 | −4.6 | 47 | −0.4 | −0.1 |
| Vector model $L = 2$ (19) | 2.8 | −0.4 | 2.9 | 1.0 | −0.1 |

$- 0.05 < g_* < 0.05$ @ 95% CL

# Constraint on 4-point function from local NG

$\tau_{NL} < 2800$ @ 95% CL

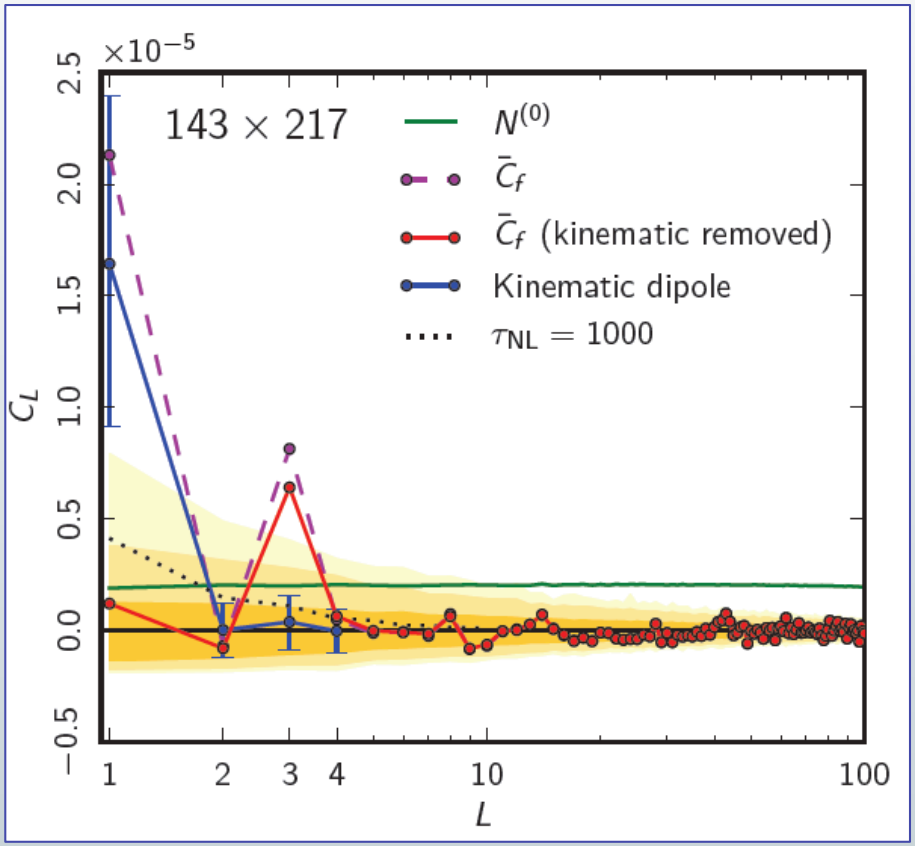


Power spectrum of the power modulation reconstructed from 143 X 217 GHz maps. Shading shows the 68%, 95% and 99% CL intervals from simulations with no modulation or kinematic signal. The dashed lines are when the mean field simulations include no kinematic eects, showing a clear detection of a modulation dipole. The blue points show the expected kinematic modulation dipole signal from simulations, along with 1σ error bars (only first four points shown for clarity). The solid line subtracts the dipolar kinematic signal in the mean fields from simulations including the expected signal, and represents out best estimate of the non-kinematic signal (note this is not just a subtraction of the power-spectra since the mean field takes out the fixed dipole anisotropy in real space before calculating the remaining modulation power). The dotted line shows the expected signal for $\tau_{NL} = 1000$.

# Conclusions I

- We have detected the Integrated-Sachs-Wolfe-lensing bispectrum atthe level expected in the ΛCDM scenario and the Poissonian point-source bispectrum contribution.

- We have derived constraints on early-Universe scenarios that generate primordial NG, including general single-field models of inflation, excited initial states (non-Bunch-Davies vacua), and directionally-dependent vector models.

- We have provided an initial survey of scale-dependent feature and resonance models. These results bound both general single-field and multi-field model parameter ranges, such as the speed of sound, $c_s \geq 0.02$ (95% CL), in an effective field theory parametrization ($c_s \geq 0.07$ *for DBI inflation*), and the curvaton decay fraction $r_D \geq 0.15$ (95% CL).

- We have constrained the amplitude of the four-point function in the local model $\tau_{NL} < 2800$ (95% CL), using an estimator introduced by Hanson & Lewis 2009, which is based on large-scale modulation of small-scale power.

# Conclusions II

- The **simplest** inflation models (single-field slow-roll, standard kinetic term, BD initial vacuum state) are favoured by *Planck* data
- Multi-field models are not ruled out but also not detected
- *Planck* data severely limit the viable parameter space of the ekpyrotic/cyclic scenarios
- *Taken together, these constraints represent the highest precision tests to date of physical mechanisms for the origin of cosmic structure.*

# Future prospects

- short term goals
  - *Improve $f_{NL}$ limits with polarization & full data*
  - *Look for more non-Gaussian shapes, scale-dependence, etc. ...*
  - *constrain $g_{NL}$*
- long terms goals
  - *reconstruct inflationary action: are models with large $g_{NL}$ and small $f_{NL}$ preferred by laws of nature?*
  - *if (quadratic) NG turns out to be small for all shapes go on and search for $f_{NL} \sim 1$ non-linear GR effects and second-order radiation transfer function contributions*
  - *what about intrinsic ($f_{NL} \sim 10^{-2}$) NG of standard inflation? CMB polarization + LSS + 21cm background + CMB spectral distortions*